

Article

Thermal Management of Concentrated Multi-Junction Solar Cells with Graphene-Enhanced Thermal Interface Materials

Mohammed Saadah ^{1,2}, Edward Hernandez ^{2,3} and Alexander A. Balandin ^{1,2,3,*}

¹ Nano-Device Laboratory (NDL), Department of Electrical and Computer Engineering, University of California, Riverside, CA 92521, USA; msaad001@ucr.edu

² Phonon Optimized Engineered Materials (POEM) Center, Bourns College of Engineering, University of California, Riverside, CA 92521, USA; ehern044@ucr.edu

³ Materials Science and Engineering Program, University of California, Riverside, CA 92521, USA

* Correspondence: balandin@ece.ucr.edu; Tel.: +1-951-827-2351

Academic Editor: Philippe Lambin

Received: 20 May 2017; Accepted: 3 June 2017; Published: 7 June 2017

Abstract: We report results of experimental investigation of temperature rise in concentrated multi-junction photovoltaic solar cells with graphene-enhanced thermal interface materials. Graphene and few-layer graphene fillers, produced by a scalable environmentally-friendly liquid-phase exfoliation technique, were incorporated into conventional thermal interface materials. Graphene-enhanced thermal interface materials have been applied between a solar cell and heat sink to improve heat dissipation. The performance of the multi-junction solar cells has been tested using an industry-standard solar simulator under a light concentration of up to 2000 suns. It was found that the application of graphene-enhanced thermal interface materials allows one to reduce the solar cell temperature and increase the open-circuit voltage. We demonstrated that the use of graphene helps in recovering a significant amount of the power loss due to solar cell overheating. The obtained results are important for the development of new technologies for thermal management of concentrated photovoltaic solar cells.

Keywords: graphene; thermal interface materials; solar cells; thermal management

1. Introduction

The interest to photovoltaic (PV) solar cells as a source of energy for a variety of applications has been rapidly increasing in recent years [1–10]. Improving solar cell performance is an important issue, and the efforts have been mostly aimed at increasing power conversion efficiency and reducing manufacturing costs. Crystalline silicon (Si) is the most commonly used material in manufacturing solar cells, occupying more than 90% of the market [10,11]. Conventional solar cells, manufactured using two-decades-old technology, are capable of converting about 20% of absorbed light energy into electricity [11,12]. Solar cell panels that employ optical concentrators can convert more than ~30% of absorbed light into electricity [13]. Most of the remaining 70% of absorbed energy is turned into heat inside the solar cell [14]. While Si PV cells remain the most common and affordable for commercial use for power generation, there is a strong motivation for development of higher efficiency multi-junction PV cells with concentrators. The concentrator multi-junction solar cells can find applications in aerospace and other technologies where efficiency and smaller size are more important considerations than cost [15].

One of the problems in developing the concentrator multi-junction PV technology is thermal management of the solar cells. Concentration of solar light into a small area, increase in the energy absorption, and layered structure of the multi-junction cells result in significant temperature increase

during the cell's operation [16]. The increase in the PV cell temperature negatively affects its power conversion efficiency, and it can damage the solar cell over time [17]. Therefore, it is important to control solar cell temperature by effectively removing the unwanted heat. Temperature effects on performance of conventional solar cells have been the subject of many reported studies [18–27]. One can distinguish two main methods of thermal management of solar cells: active cooling and passive cooling. The active cooling involves a cooling medium, e.g., air or water, and uses fans or water pumps to push the medium through the heated surfaces. Passive cooling uses a heat sink that dissipates heat without pushing a cooling medium through it. Most solar cells utilize passive cooling technologies [28,29]. A basic heat sink can reduce the temperature of a standard Si solar cell, under one sun illumination, by about 15 °C, which increases the output power by 6% [30]. When a heat sink is attached to a solar cell, a thermal resistance between the two interfaces can limit the amount of heat transferred between the solar cell and the heat sink [31]. This resistance is a result of small air gaps between the two joined surfaces, which are caused by the surfaces microscopic imperfections [32]. Since air is a poor thermal conductor, it must be replaced by a material that has better thermal conductivity (see Figure 1). The thickness of this material, referred to as bond line thickness (BLT), should be kept small to minimize the overall thermal resistance of the connected surfaces. One should note that, even if the joined surfaces are polished to perfection, the thermal boundary resistance (TBR) will still exist at the interface of two materials owing to the mismatch in their acoustic phonon properties. Thermal interface materials (TIMs) or thermal phase change materials (PCMs) perform the task of reducing thermal resistance between two surfaces and facilitating heat transfer between the heat generating device and a heat sink [33–40].

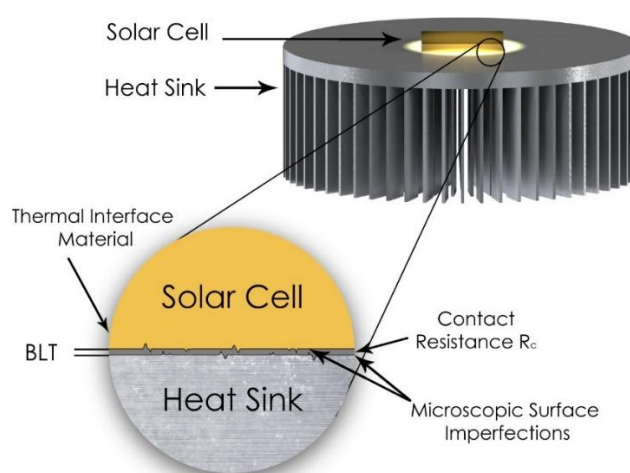


Figure 1. Illustration of the function of the thermal interface materials for heat removal from the solar cell under concentrated light.

In this paper, we demonstrate that the thermal management of concentrator multi-junction solar cells can be substantially improved by enhancing properties of TIMs via incorporation of graphene [41]. Conventional TIMs are typically made of polymeric or grease base material loaded with conductive materials such as silver or ceramic particles [42]. The amount of various fillers in the commercial TIMs can be high, reaching the loading volume fractions $f \sim 70\%$ [43]. The approach of increasing the filler loading fraction f for higher thermal conductivity of the resulting composite has limitations. Higher loadings may result in the uneven dispersion of the fillers, their agglomeration, air gaps, and increases in the TIM cost [44,45]. Our results indicate that the use of low loading fractions of graphene as an additional filler to commercial TIMs can be an effective strategy for decreasing the operation temperature of multi-junction PV cells under high concentrations of solar energy.

Graphene is a single layer of carbon atoms that are strongly bonded in a hexagonal honeycomb lattice. This material has proven to have an unusually high thermal conductivity with intrinsic values

in the range of 2000 to 5000 W/mK near room temperature [46]. This is an order of magnitude larger than pure silver [33–35]. The thermal conductivity of graphene flakes reduces with decreasing lateral dimensions of the flakes and upon contact with the base or matrix material. However, it still remains high compared to many other filler materials used previously. It has been found that there is an optimum distribution of graphene fillers in terms of their size and thickness [45]. Few-layer graphene (FLG) flakes can be more efficient as fillers because their thermal conductivity is less subject to degradation upon surface exposure to the base material of the composite [43,45]. However, when FLG thickness becomes too large, the thermal coupling of the fillers to the base material may suffer. From these considerations, one should determine the optimum FLG characteristics for a given base material, range of the loading, and applications. Given a strong current interest to the concentrator solar cells [47–55] and the problems with their thermal management, in this work we examine a feasibility of using graphene and FLG fillers for heat removal from advanced photovoltaic solar cells.

2. Material Preparation and Characterization

The thermal composites tested in this research were prepared from several common commercial TIMs (e.g., “Ice Fusion” and “Arctic Alumina”). These composite materials use silver, aluminum oxide, and aluminum nitrite particles—or combinations of thereof—as fillers to enhance the thermal conductivity of TIM. As an additional filler, we have utilized commercial liquid phase exfoliated (LPE) graphene and FLG mixture (Graphene Supermarket, Graphene Laboratories Inc., Calverton, NY, USA). The mixture had a large concentration of FGL flakes with the thickness between three and eight monolayers (total thickness below 3 nm) and lateral dimension in the range of 2–8 μm . The quality of material has been verified with Raman spectroscopy, optical and scanning electron microscopy (SEM) following the procedures reported by some of us earlier [41,43,45]. One should note that LPE is a scalable method for producing inexpensive graphene—FLG solution with the quality sufficient for thermal applications. We used a microscale to weigh the TIM and LPE graphene with $\pm 0.01\%$ accuracy. The mixture of commercial TIMs with added graphene fillers was placed in a vial to the two-axis rotating mixer. The composite was mixed at 2500 rpm for three minutes. A vacuum pump was used to eliminate the bubbles in the composite for two minutes. This mixing and vacuuming process was repeated three to four times to ensure uniform filler dispersion with minimum concentration and size of air pockets. The percentage of additional graphene fillers in TIMs is calculated as $\text{wt } \% = W_g / (W_B + W_g)$, where W_g and W_B are the weights of graphene—FLG fillers and base material, respectively. In this case, the base material is the initial commercial TIM. The volume loading fraction of graphene fillers was determined from the equation: $\text{vol } \% = (W_g / \rho_g) / ((W_g / \rho_g) + (W_B / \rho_B))$, where ρ_g and ρ_B are the mass density of graphene and base material, respectively.

In order to make sure that addition of graphene—FLG fillers was done successfully and the thermal conductivity of TIMs increased, we conducted measurements of the apparent thermal conductivity of the resulting composite between two metal plates. The measurements were conducted using the industry standard TIM tester method (Analysis Tech TIM Tester, Boston, MA, USA) with the software-controlled contact pressure and temperature. The electronic ‘in situ thickness measurement’ function provided accurate values of the thickness of the composite layer for further analysis. It is important to note here that the TIM tester values of the apparent thermal conductivity are lower than the bulk values owing to the effect of the thermal resistance with the contacting surfaces. However, the TIM tester thermal conductivity is more relevant for practical applications of TIMs. Figure 2 shows representative results of the thermal measurements for two commercial TIMs with added graphene fillers. The thermal conductivity data are presented for graphene filler loading of up to 6 wt %. The sample temperature was fixed at 50 $^{\circ}\text{C}$ while the pressure maintained at 100 kPa. One can see that, in one composite, the thermal conductivity increases by 130% as compared to commercial TIM without extra graphene fillers. In another composite, the thermal conductivity increases by 77% and starts to saturate gradually for the loading fractions above 4 wt %. It is interesting to note that a stronger enhancement due to graphene was observed in the least expensive commercial TIM. The fact that higher loading fraction of additional graphene fillers does not improve

thermal conductivity of some TIMs is not surprising. Commercial TIMs already have high loading of other fillers and the addition of graphene fillers above certain fraction (~4 wt % in this case) can degrade viscosity and other parameters. For these reasons, in our solar cell testing, we used commercial TIMs enhanced with graphene fillers of the loading fraction of up to 4 wt %. The low loading of graphene is also beneficial from the practical material cost considerations.

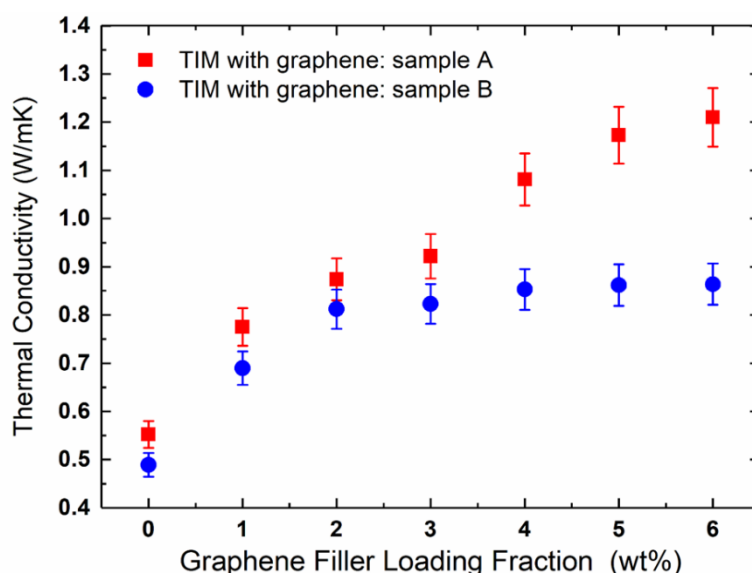


Figure 2. Measured apparent thermal conductivity of two representative commercial thermal interface materials, denoted as “sample A” and “sample B”, with added graphene fillers. The data are presented as a function of the graphene loading weight fraction. The measurements were conducted at $T = 50\text{ }^{\circ}\text{C}$ and pressure of 100 kPa. Note that the apparent thermal conductivity values include the effects of the thermal contact resistance.

In the present and previous studies of graphene-enhanced TIMs, we verified that mixing and vacuuming of commercial TIMs without addition of graphene have not improved their thermal conductivity [34,37,41,43]. These tests have been performed to establish that graphene fillers are responsible for the improved apparent thermal conductivity rather than additional mixing and vacuuming processing steps by themselves. At the small loading fractions used, graphene fillers are not forming the percolation network as confirmed by the microscopy and electrical resistivity measurements [41,43,45]. The increase in the thermal conductivity of the resulting composite can come owing to two possible mechanisms. The first one is related to very high intrinsic thermal conductivity of graphene [46] and its good coupling to the matrix materials [41,43,45]. The heat propagates partially via graphene fillers and partially via the matrix material. Even if the thermal conductivity of graphene–FLG fillers is reduced due to the exposure to the matrix, the effective medium approximation (EMA) predicts a large increase in the thermal conductivity of the composite (larger than the measured one) [45]. The second possible mechanism of enhancement is the action of graphene fillers as connecting thermal links among existing larger scale fillers in the commercial TIMs. Such a mechanism has been known and studied for other fillers with different aspect ratios, e.g., spherical metal particles and carbon nanotubes [56,57].

3. Testing of the Photovoltaic Solar Cells

To investigate the effects of graphene fillers on the performance of TIMs with the concentrated photovoltaic solar cells, we applied graphene-enhanced TIMs between the solar cell (acting as a heat source) and an aluminum heat sink (see Figure 1). The TIM layer enhances the thermal contact between the two surfaces by replacing the air gaps with thermally conductive paste. The pressure between the two surfaces was fixed at 100 kPa in all measurements. The TIM function is reducing the

thermal resistance, R_{TIM} , between two adjoining surfaces. This resistance is affected by several factors, including TIM thermal conductivity, K_{TIM} , thermal contact resistances, R_c , between the TIM layer and the two surfaces, and the distance between the two surfaces or BLT . These factors are related to R_{TIM} by the equation

$$R_{TIM} = \frac{BLT}{K_{TIM}} + R_{c1} + R_{c2} \quad (1)$$

The graphene enhanced TIMs and reference TIMs without graphene were carefully spread on the back surface of the solar cell panels to ensure uniform and complete coverage, and to avoid excessive amount of material, which would negatively affect R_{TIM} via large BLT (see Equation (1)). Figure 3 shows the back side of the solar cell with TIM before and after the attachment of two surfaces.

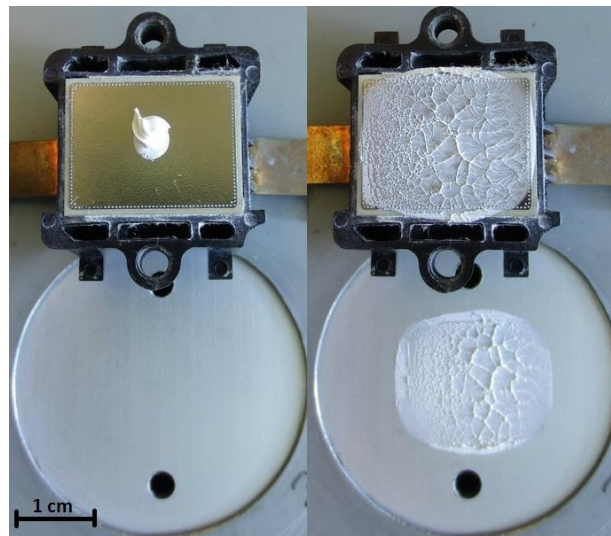


Figure 3. Image of the actual photovoltaic cells with the dispersed thermal interface material.

The photovoltaic solar cell with different TIMs has been tested by placing it under a solar simulator (Sol1A Class, Newport Corporation, in Irvine, CA, USA) as shown in Figure 4. The solar simulator uses a xenon lamp that produces a $6 \times 6''$ size beam that emits the 5800 K blackbody-like spectrum. The simulator uses a special power supply to maintain a strictly constant level of illumination. The light produced by the xenon lamp is reflected by a mirror to pass through a spectral correction filter that simulate the AM1.5 G solar spectra. The light beam then passes through a collimating lens that emulate the 0.5° angle that the sun light has when it reaches the earth. The open circuit voltage is recorded every second using a voltage logger and the temperature of the solar cell is measured using a multi-channel temperature logger. A large convex lens is placed between the solar simulator and solar cell. By varying the distance between the lens and the solar cell, one increases or decreases the light concentration on the solar cell (simulating 500–2000 suns). In high concentration experiments we employed two lenses: a large convex lens and a small lens placed on the solar cell. All experiments were taken at a room temperature of $25^\circ\text{C} (\pm 2^\circ\text{C})$.

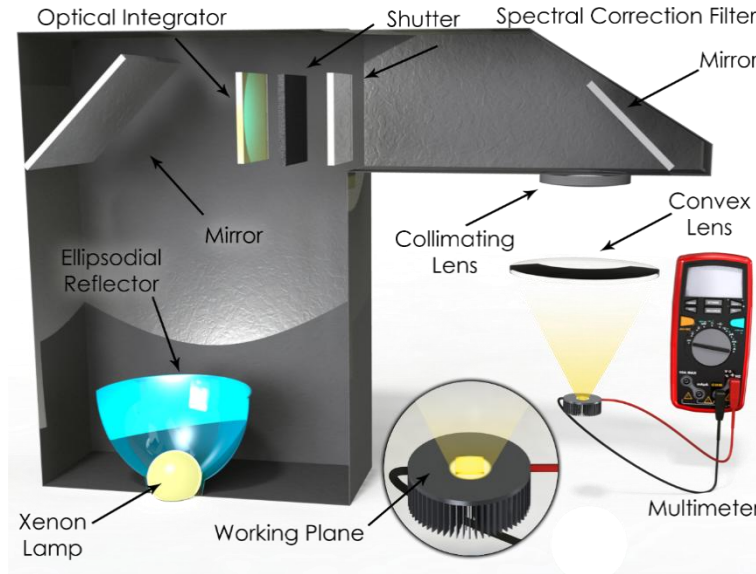


Figure 4. Schematic of the testing procedures for solar cells attached to the heat sink. The lenses allowed to test the performance under concentrated light conditions corresponding to up to 2000 suns.

4. Results and Discussion

Before presenting the results of the tests, we briefly outline the expected effects of temperature on the PV cell performance from the theoretical point of view. The increase in temperature leads to a decrease in the band gap energy, E_g , of a semiconductor [3]

$$E_g(T) = E_g(0) - \frac{\alpha T^2}{T + \beta} \quad (2)$$

Here $E_g(T)$ is the band gap of a semiconductor at temperature T , α and β are material constants, and $E_g(0)$ is the band gap value at zero Kelvin. The decrease in the band gap leads to a slight increase in the short-circuit current, I_{sc} , owing to the enhanced absorption and photocurrent. However, the heating results in a more pronounced detrimental effect on the open-circuit voltage, V_{oc} , defined as the maximum voltage when the PV cell is open and zero current is flowing. The open-circuit voltage is given as [3]

$$V_{oc} = \frac{kT}{q} \ln\left(\frac{I_{sc}}{I_0} + 1\right) \quad (3)$$

where I_0 is the reverse saturation current, q is electron charge, and k is the Boltzmann constant.

Many parameters in equations governing PV cell performance depend on temperature, including band gap, diffusion coefficients, built-in voltage, intrinsic carrier concentration, and depletion region width. It is challenging to disentangle the effect of temperature on each of them term by term. However, computational studies for different material systems predict a linear decrease in the open-circuit voltage and the fill factor (FF), slightly offset by the linear increase in the short-circuit current. The result of these trends is a linear decrease in the power conversion efficiency, η , which determines how much of the input solar energy is converted into electricity

$$\eta = \frac{P_{mp}}{P_{in}} = \frac{FF \cdot I_{sc} V_{oc}}{P_{in}} \quad (4)$$

Here, the maximum power output, P_{mp} , corresponds to the point in the current-voltage characteristic where the current is at maximum, I_{mp} , and voltage, V_{mp} , is maximum. These parameters define the fill factor: $FF = I_{mp} V_{mp} / (I_{sc} V_{oc}) = P_{mp} / (I_{sc} V_{oc})$. For crystalline Si, FF is in the range of 0.7 to 0.85, and the efficiency ranges from 13% to 16%. According to the theory, the maximum power output for crystalline solar cell decreases by 0.4%–0.5% per every 1 °C increase in the cell temperature [58–61].

Based on these theory considerations, we focus on investigation of the temperature effects on open-circuit voltage, V_{oc} , and then calculate the change in the efficiency, η . The first experimental runs have been conducted for a single junction large area polycrystalline Si solar panel in order to better elucidate the effects of solar cell panel overheating. No special heat sink or TIM have been used. Figure 5 shows the temperature effect on V_{oc} of the panel placed under the solar simulator. In the first 10 min we see a decrease in the open circuit voltage, V_{oc} , as the temperature of the solar cell panel increases from 25 to 55 °C. The 30 °C temperature rise results in the V_{oc} change of about 12%. At the next step, the solar simulator is shut off for the next 10 min leaving the solar cell panel without illumination. The non-zero V_{oc} in time period from 10 to 20 min is the panel output due to ambient light in the laboratory. As the solar cell temperature decreases to RT ($T = 25$ °C) the open-circuit voltage gradually increases. This cycle is repeated again verifying reproducibility of the results. The measured decrease in the output power is around 0.4% per 1 °C increase in cell temperature, which is close to the theoretical values [62]. Based on these experiments, we can conclude that our measurement procedures and protocols are proper for the intended study.

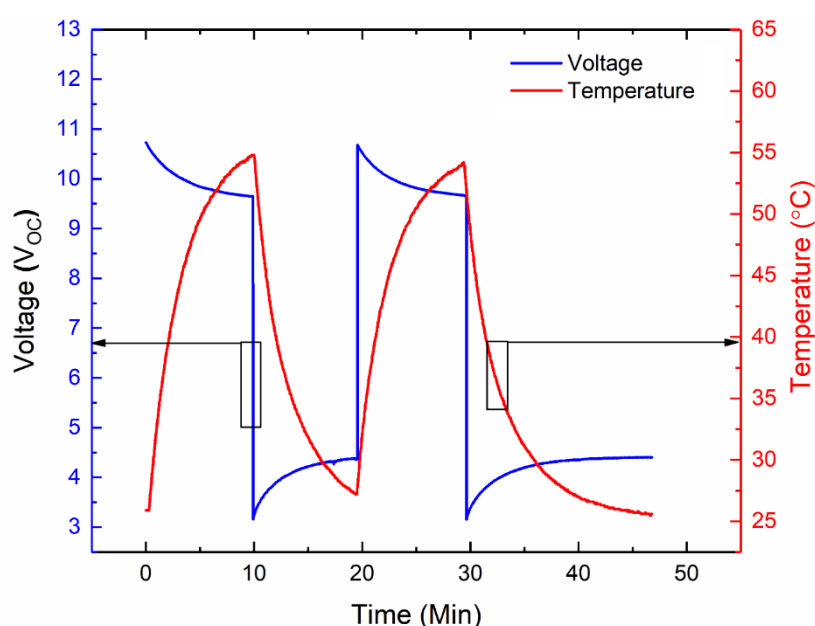


Figure 5. Open-circuit voltage and the cell temperature as the functions of time for the multi-junction solar cell under one sun illumination. The increase in the cell temperature under illumination results in the corresponding decrease in the open-circuit voltage.

We now turn to the small-area multi-junction solar cell (InGaP/InGaAs/Ge triple-junction SC) and verify that the light concentration function properly. The solar cell without a heat sink was illuminated with the concentrated light corresponding to 500, 1000, 1500 and 2000 suns (see Figure 6). At the moment of switching on the illumination the open-circuit voltage, V_{oc} , was 2.75, 3.15, 3.35 and 3.65 V under 500, 1000, 1500 and 2000 suns, respectively. The open-circuit voltage increases with the increasing concentration as expected. After just a few minutes of illumination, the V_{oc} value decreases by 29%–34% owing to heating of the solar cell. Increasing the light concentration resulted in small linear increase in the short-circuit current. Figure 7 shows that the short-circuit current, I_{sc} , increases slightly with increasing temperature (about 1%). This increase in I_{sc} cannot compensate for the decrease in V_{oc} . Overall, the current scales up with increasing the light concentration. The output power of the multi-junction solar cell decreases with time owing to the sharp drop of the open-circuit voltage. These results further demonstrate the importance of thermal management of multi-junction solar cells under highly concentrated illumination.

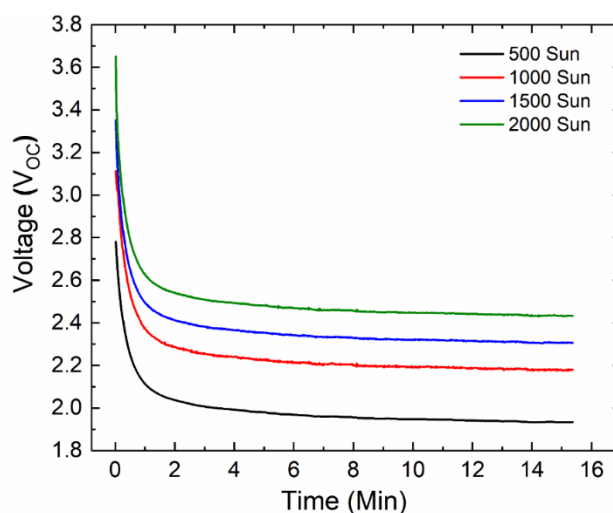


Figure 6. Open-circuit voltage as the function of time for the multi-junction solar cell under concentrated illumination corresponding to 500, 1000, 1500, and 2000 suns.

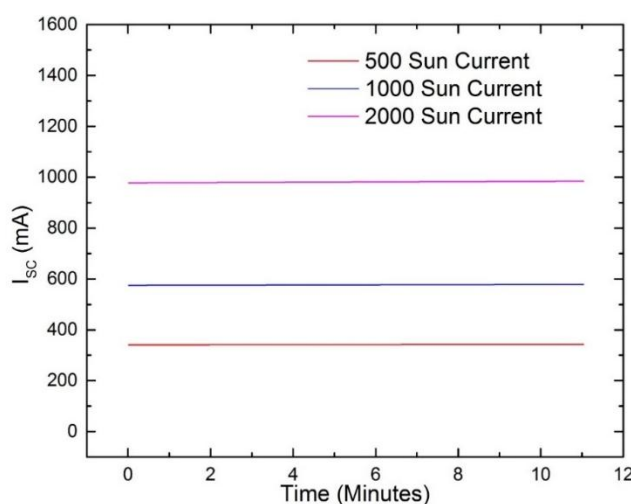


Figure 7. Short-circuit current as the function of time for the multi-junction solar cell under concentrated illumination corresponding to 500, 1000, 1500 and 2000 suns.

To prevent or reduce the power loss, we attached the multi-junction solar cell to an aluminum heat sink with the graphene-enhanced TIMs. For comparison, we also run experiments for the solar cell on a heat sink without TIM and on a heat sink with commercial TIM. Figure 8 shows V_{oc} of the multi-junction solar cell under 1000 sun concentrated light. One can see a significant positive effect of additional graphene fillers for heat removal from the cell. The decrease in voltage becomes less than 12% when TIM with 4 wt % of graphene is used as compared to 29% decrease in the cell operating without TIM. This translates to recovery of about 60% of the power loss. Figure 9 presents results for the same type of testing but with the 2000 sun light concentration. One can see that the open-circuit voltage drop went from 0.9 V in case of 1000 suns to 1.2 V for 2000 sun concentration due to overheating. The use of the graphene enhanced TIMs allows one to decrease the V_{oc} degradation from 34% to about 12% of the initial value. This constitutes a recovery of about 65% of the energy lost due to overheating. In both cases, TIMs with graphene perform substantially better than conventional commercial TIMs. It is also important to note that improvement in TIMs performance comes at a very low loading fraction of graphene.

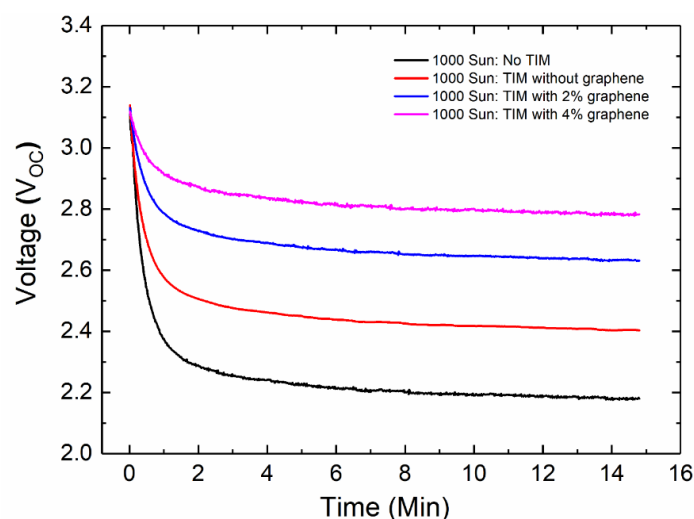


Figure 8. Open-circuit voltage of the solar cell under concentrated illumination corresponding to 1000 suns. The results are shown for the cell without thermal interface material, for the same cell with commercial thermal interface materials, and for the same cell with graphene-enhanced thermal interface materials. Note that the use of 4% graphene fillers added to commercial thermal paste allows for substantial increase in the open-circuit voltage.

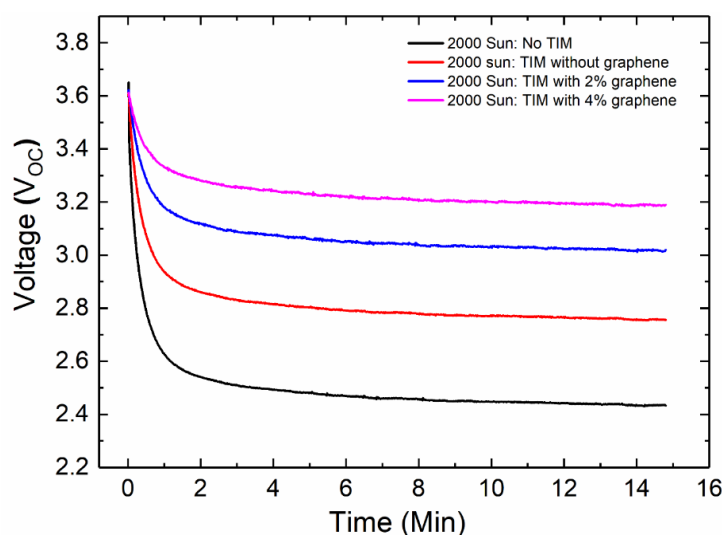


Figure 9. Open-circuit voltage of the solar cell under concentrated illumination corresponding to 2000 suns. The results are shown for the cell without thermal interface material, for the same cell with commercial thermal interface materials, and for the same cell with graphene-enhanced thermal interface materials. Note that the use of 4% graphene fillers added to commercial thermal paste allows for substantial increase in the open-circuit voltage.

The obtained values for reduction in the temperature of the cell and saved output power are specific for the tested multi-junction cell and depend on many parameters, e.g., the heat sink used, ambient temperature cell design, and others. The performance of graphene-enhanced TIMs with other PV cells may vary. The present research succeeded in demonstration of a principal possibility of decreasing the PV cell temperature with commercial TIMs enhanced with a small loading fraction of LPE graphene. Our proposed method can complement the existing technologies for passive thermal management of solar cells [63,64], particularly for the countries with a high average temperature, and contribute to the development of more sustainable approaches of energy supply [65].

5. Conclusions

We reported results of an investigation of temperature increase in concentrated multi-junction solar cells with thermal interface materials enhanced by addition of a small loading fraction (below 4 wt %) of graphene. Graphene and few-layer graphene fillers, produced by a scalable liquid-phase exfoliation technique, were incorporated into commercial thermal interface materials. Graphene-enhanced thermal interface materials have been applied between a solar cell and heat sink to improve heat dissipation. It was found that the application of graphene-enhanced thermal interface materials allows one to reduce the solar cell temperature and increase the open-circuit voltage. Graphene fillers help in recovering a significant amount of power loss due to overheating. The obtained results can lead to the development of new technologies for thermal management of concentrated photovoltaic solar cells.

Acknowledgments: Mohammed Saadah acknowledges financial support for his dissertation research at UC Riverside from The King Abdullah Scholarship Program (KASP) and the Saudi Arabian Cultural Mission, Los Angeles, CA, USA. Alexander A. Balandin acknowledges partial support from the National Science Foundation (NSF) awards 1404967 and 1549942.

Author Contributions: Mohammed Saadah prepared the composites, conducted photovoltaic solar cell testing and processed the experimental data; Edward Hernandez assisted with thermal measurements and solar cell testing. Alexander A. Balandin coordinated the project, contributed to data analysis. Mohammed Saadah and Alexander A. Balandin wrote the manuscript. Edward Hernandez created original art figures 1 and 4.

Conflicts of Interest: The authors declare no conflict of interest.

References

1. Sohrabi, F.; Nikniazi, A.; Movla, H. *Optimization of Third Generation Nanostructured Silicon-Based Solar Cells. In Solar Cells—Research and Application Perspectives*; Morales-Acevedo, A., Ed.; In Tech: Rijeka, Croatia, 2013; pp. 1–26.
2. Nalwa, H.S. *Encyclopedia of Nanoscience and Nanotechnology*; American Scientific Publishers: California, CA, USA, 2004; pp. 727.
3. Masuko, K.; Shigematsu, M.; Hashiguchi, T.; Fujishima, D.; Kai, M.; Yoshimura, N.; Yamaguchi, T.; Ichihashi, Y.; Mishima, T.; Matsubara, N.; et al. Achievement of More Than 25% Conversion Efficiency With Crystalline Silicon Heterojunction Solar Cell. *Photovoltaics, IEEE J.* **2014**, *4*, 1433–1435. doi:10.1109/JPHOTOV.2014.2352151.
4. Van Sark, W.; Korte, L.; Roca, F. *Introduction—Physics and Technology of Amorphous-Crystalline Heterostructure Silicon. In Physics and Technology Amorphous-Crystalline Heterostructure Silicon Solar Cells*; Springer-Verlag: Berlin/Heidelberg, Germany, 2012; pp. 1–12. doi:10.1007/978-3-642-22275-7.
5. Glunz, S.W. High-efficiency crystalline silicon solar cells. *Adv. Optoelectron.* **2007**. doi:10.1155/2007/97370.
6. Snaith, H.J. Perovskites: The Emergence of a New Era for Low-Cost, High-Efficiency Solar Cells. *J. Phys. Chem. Lett.* **2013**, *4*, 3623–3630. doi:10.1021/jz4020162.
7. Becker, C.; Amkreutz, D.; Sontheimer, T.; Preidel, V.; Lockau, D.; Haschke, J.; Jogschies, L.; Klimm, C.; Merkel, J.J.; Plocica, P.; et al. Polycrystalline silicon thin-film solar cells: Status and perspectives. *Sol. Energy Mater. Sol. Cells.* **2013**, *119*, 112–123. doi:10.1016/j.solmat.2013.05.043.
8. Konagai, M. Present status and future prospects of silicon thin-film solar cells. *Jpn. J. Appl. Phys.* **2011**, *50*. doi:10.1143/JJAP.50.030001.
9. Avrutin, V.; Izyumskaya, N.; Morko, H. Semiconductor solar cells: Recent progress in terrestrial applications. *Superlattices Microstruct.* **2011**, *49*, 337–364. doi:10.1016/j.spmi.2010.12.011.
10. Tyagi, V.V.; Rahim, N.A.A.; Rahim, N.A.; Selvaraj, J.A.L. Progress in solar PV technology: Research and achievement. *Renew. Sustain. Energy Rev.* **2013**, *20*, 443–461. doi:10.1016/j.rser.2012.09.028.
11. Lee, H.S. *Thermal Design: Heat Sinks, Thermoelectrics, Heat Pipes, Compact Heat Exchangers, and Solar Cells*; John Wiley & Sons: New York, NY, USA, 2010; pp. 482. doi:10.1002/9780470949979.
12. Green, M.A.; Emery, Y.; Hishikawa, W.; Warta, E.D. Dunlop, Solar cell efficiency tables (version 47). *Prog. Photovolt. Res. Appl.* **2016**, *24*, 3–11. doi:10.1002/pip.2728.
13. Xie, W.T.; Dai, Y.J.; Wang, R.Z.; Sumathy, K. Concentrated solar energy applications using Fresnel lenses: A review. *Renew. Sustain. Energy Rev.* **2011**, *15*, 2588–2606. doi:10.1016/j.rser.2011.03.031.

14. Huang, B.J.; Yang, P.E.; Lin, Y.P.; Lin, B.Y.; Chen, H.J.; Lai, R.C.; Cheng, J.S. Solar cell junction temperature measurement of PV module. *Sol. Energy*. **2011**, *85*. doi:10.1016/j.solener.2010.11.006.
15. McConnell, R.; Symko-Davies, M. Multijunction photovoltaic technologies for high-performance concentrators. In Proceedings of the Conference Record of the 2006 IEEE 4th World Conference on Photovoltaic Energy Conversion (WCPEC-4), Waikoloa, HI, USA, 7–12 May 2006; pp. 733–736. doi:10.1109/WCPEC.2006.279560.
16. Baig, H.; Heasman, K.C.; Mallick, T.K. Non-uniform illumination in concentrating solar cells. *Renew. Sustain. Energy Rev.* **2012**, *16*, 5890–5909. doi:10.1016/j.rser.2012.06.020.
17. Saga, T. Advances in crystalline silicon solar cell technology for industrial mass production. *NPG Asia Mater.* **2010**, *2*, 96–102. doi:10.1038/asiamat.2010.82.
18. Chander, S.; Purohit, A.; Sharma, A.; Arvind; Nehra, S.P.; Dhaka, M.S. A study on photovoltaic parameters of mono-crystalline silicon solar cell with cell temperature. *Energy Rep.* **2015**, *1*, 104–109. doi:10.1016/j.egy.2015.03.004.
19. Rahman, M.M.; Hasanuzzaman, M.; Rahim, N.A. Effects of various parameters on PV-module power and efficiency. *Energy Convers. Manag.* **2015**, *103*, 348–358. doi:10.1016/j.enconman.2015.06.067.
20. Meneses-Rodríguez, D.; Horley, P.P.; González-Hernández, J.; Vorobiev, Y.V.; Gorley, P.N. Photovoltaic solar cells performance at elevated temperatures. *Sol. Energy* **2005**, *78*, 243–250. doi:10.1016/j.solener.2004.05.016.
21. Radziemska, E. Thermal performance of Si and GaAs based solar cells and modules: A review. *Prog. Energy Combust. Sci.* **2003**, *29*, 407–424. doi:10.1016/S0360-1285(03)00032-7.
22. Skoplaki, E.; Palyvos, J.A. On the temperature dependence of photovoltaic module electrical performance: A review of efficiency/power correlations. *Sol. Energy* **2009**, *83*, 614–624. doi:10.1016/j.solener.2008.10.008.
23. El-Adawi, M.K.; Al-Nuaim, I.A. The temperature functional dependence of V_{oc} for a solar cell in relation to its efficiency new approach. *Desalination* **2007**, *209*, 91–96. doi:10.1016/j.desal.2007.04.014.
24. Radziemska, E.; Klugmann, E. Thermally affected parameters of the current-voltage characteristics of silicon photocell. *Energy Convers. Manag.* **2002**, *43*, 1889–1900. doi:10.1016/S0196-8904(01)00132-7.
25. Cuce, E.; Bali, T. Variation of cell parameters of a p-Si PV cell with different solar irradiances and cell temperatures in humid climates. In Proceedings of the 4th International Energy, Exergy and Environment Symposium, Sharjah, UAE, 19–23 April 2009.
26. Cuce, E.; Bal, T. A Comparison of Energy and Power Conversion Efficiencies of m-Si and p-Si PV Cells in Trabzon. In Proceedings of the 5th International Advanced Technologies Symposium, Karabuk, Turkey, 15–19 May 2009.
27. Natarajan, S.K.; Mallick, T.K.; Katz, M.; Weingaertner, S. Numerical investigations of solar cell temperature for photovoltaic concentrator system with and without passive cooling arrangements. *Int. J. Therm. Sci.* **2011**, *50*, 2514–2521. doi:10.1016/j.ijthermalsci.2011.06.014.
28. Ye, Z.; Li, Q.; Zhu, Q.; Pan, W. The cooling technology of solar cells under concentrated system. In Proceedings of the 2009 IEEE 6th International Power Electronics and Motion Control Conference (IPEMC'09), Wuhan, China, 17–20 May 2009; pp. 2193–2197. doi:10.1109/IPEMC.2009.5157766.
29. Bojanampati, S.; Rodgers, P. Experimental assessment of flat-type photovoltaic module thermal behavior. In Proceedings of the 13th International Conference on Thermal, Mechanical and Multi-Physics Simulation and Experiments in Microelectronics and Microsystems (EuroSimE), Cascais, Portugal, 16–18 April 2012. doi:10.1109/ESimE.2012.6191695.
30. Tong, X.C. Advanced Materials for Thermal Management of Electronic Packaging. *Adv. Mater.* **2011**, *30*, 201–232. doi:10.1007/978-1-4419-7759-5.
31. Gwinn, J.P.; Webb, R.L. Performance and testing of thermal interface materials. *Microelectron. J.* **2003**, *34*, 215–222. doi:10.1016/S0026-2692(02)00191-X.
32. Prasher, R. Thermal Interface Materials: Historical Perspective, Status, and Future Directions. *Proc. IEEE* **2006**, *94*, 1571–1586. doi:10.1109/JPROC.2006.879796.
33. Renteria, J.D.; Nika, D.L.; Balandin, A.A. Graphene Thermal Properties: Applications in Thermal Management and Energy Storage. *Appl. Sci.* **2014**, *4*, 525–547. doi:10.3390/app4040525.
34. Goli, P.; Legedza, S.; Dhar, A.; Salgado, R.; Renteria, J.; Balandin, A.A. Graphene-enhanced hybrid phase change materials for thermal management of Li-ion batteries. *J. Power Sources* **2014**, *248*, 37–43. doi:10.1016/j.jpowsour.2013.08.135.

35. Yan, Z.; Nika, D.L.; Balandin, A.A. Special Issue on Graphene Electronics Thermal properties of graphene and few-layer graphene: Applications in electronics. *IET Circuits Devices Syst.* **2014**, *9*, 4–12. doi:10.1049/iet-cds.2014.0093.
36. Malekpour, H.; Chang, K.H.; Chen, J.C.; Lu, C.Y.; Nika, D.L.; Novoselov, K.S.; Balandin, A.A. Thermal conductivity of graphene laminate. *Nano Lett.* **2014**, *14*, 5155–5161. doi:10.1021/nl501996v.
37. Renteria, J.; Legedza, S.; Salgado, R.; Balandin, M.P.; Ramirez, S.; Saadah, M.; Kargar, F.; Balandin, A.A. Magnetically-functionalized self-aligning graphene fillers for high-efficiency thermal management applications. *Mater. Des.* **2015**, *88*, 214–221. doi:10.1016/j.matdes.2015.08.135.
38. Khandelwal, R.; Kishen, J.M.C. Thermal weight functions for bi-material interface crack system using energy principles. *Int. J. Solids Struct.* **2008**, *45*, 6157–6176. doi:10.1016/j.ijsolstr.2008.07.013.
39. Memon, M.O.; Haillot, S.; Lafdi, K. Carbon nanofiber based buckypaper used as a thermal interface material. *Carbon* **2011**, *49*, 3820–3828. doi:10.1016/j.carbon.2011.05.015.
40. Li, X.; Yang, R. Effect of lattice mismatch on phonon transmission and interface thermal conductance across dissimilar material interfaces. *Phys. Rev. B Condens. Matter Mater. Phys.* **2012**, *86*. doi:10.1103/PhysRevB.86.054305.
41. Shahil, K.M.F.; Balandin, A.A. Thermal properties of graphene and multilayer graphene: Applications in thermal interface materials. *Solid State Commun.* **2012**, *152*, 1331–1340. doi:10.1016/j.ssc.2012.04.034.
42. Sarvar, F.; Whalley, D.; Conway, P. Thermal Interface Materials—A Review of the State of the Art. In Proceedings of the 2006 1st Electronics Systemintegration Technology Conference, Dresden, Germany, 5–7 September 2006; pp. 1292–1302. doi:10.1109/ESTC.2006.280178.
43. Goyal, V.; Balandin, A.A. Thermal properties of the hybrid graphene-metal nano-micro-composites: Applications in thermal interface materials. *Appl. Phys. Lett.* **2012**, *100*, 073113. doi:10.1063/1.3687173.
44. McNamara, A.J.; Joshi, Y.; Zhang, Z.M. Characterization of nanostructured thermal interface materials—A review. *Int. J. Therm. Sci.* **2012**, *62*, 2–11. doi:10.1016/j.ijthermalsci.2011.10.014.
45. Shahil, K.M.F.; Balandin, A.A. Graphene-multilayer graphene nanocomposites as highly efficient thermal interface materials. *Nano Lett.* **2012**, *12*, 861–867. doi:10.1021/nl203906r.
46. Nika, D.L.; Balandin, A.A. Phonons and thermal transport in graphene and graphene-based materials. *Rep. Prog. Phys.* **2017**, *80*, 36502. doi:10.1088/1361-6633/80/3/036502.
47. Guter, W.; Schöne, J.; Philipps, S.P.; Steiner, M.; Siefer, G.; Wekkeli, A.; Welser, E.; Oliva, E.; Bett, A.W.; Dimroth, F. Current-matched triple-junction solar cell reaching 41.1% conversion efficiency under concentrated sunlight. *Appl. Phys. Lett.* **2009**, *94*. doi:10.1063/1.3148341.
48. Dimroth, F.; Grave, M.; Beutel, P.; Fiedeler, U.; Karcher, C.; Tibbits, T.N.D.; Oliva, E.; Siefer, G.; Schachtner, M.; Wekkeli, A.; et al. Wafer bonded four-junction GaInP/GaAs//GaInAsP/GaInAs concentrator solar cells with 44.7% efficiency. *Prog. Photovolt. Res. Appl.* **2014**, *22*, 277–282. doi:10.1002/pip.2475.
49. Dahal, R.; Li, J.; Aryal, K.; Lin, J.Y.; Jiang, H.X. InGaN/GaN multiple quantum well concentrator solar cells. *Appl. Phys. Lett.* **2010**, *97*. doi:10.1063/1.3481424.
50. Wheeldon, J.F.; Valdivia, C.E.; Walker, A.W.; Kolhatkar, G.; Jaouad, A.; Turala, A.; Riel, B.; Masson, D.; Puetz, N.; Fafard, S.; et al. Performance comparison of AlGaAs, GaAs and InGaP tunnel junctions for concentrated multijunction solar cells. *Prog. Photovolt. Res. Appl.* **2011**, *19*, 442–452. doi:10.1002/pip.1056.
51. Lee, S. Thermal challenges and opportunities in concentrated photovoltaics. In Proceedings of the 12th Electronics Packaging Technology Conference (EPTC), Singapore, 8–10 December 2010; pp. 608–613. doi:10.1109/EPTC.2010.5702711.
52. Buljan, M.; Mendes-Lopes, J.; Benítez, P.; Miñano, J.C. Recent trends in concentrated photovoltaics concentrators' architecture. *J. Photonics Energy* **2014**, *4*, 40995. doi:10.1117/1.JPE.4.040995.
53. Tromholt, T.; Katz, E.A.; Hirsch, B.; Vossier, A.; Krebs, F.C. Effects of concentrated sunlight on organic photovoltaics. *Appl. Phys. Lett.* **2010**, *96*. doi:10.1063/1.3298742.
54. Barlev, D.; Vidu, R.; Stroeve, P. Innovation in concentrated solar power. *Sol. Energy Mater. Sol. Cells* **2011**, *95*, 2703–2725. doi:10.1016/j.solmat.2011.05.020.
55. Chemisana, D. Building integrated concentrating photovoltaics: A review. *Renew. Sustain. Energy Rev.* **2011**, *15*, 603–611. doi:10.1016/j.rser.2010.07.017.
56. Gulotty, R.; Castellino, M.; Jagdale, P.; Tagliaferro, A.; Balandin, A.A. Effects of Functionalization on Thermal Properties of Single-Wall and Nanotube À Polymer Nanocomposites. *ACS Nano*. **2013**, *7*, 5114–5121. doi:10.1021/Nn400726g.

57. Ramirez, S.; Chan, K.; Hernandez, R.; Recinos, E.; Hernandez, E.; Salgado, R.; Khitun, A.G.; Garay, J.E.; Balandin, A.A. Thermal and magnetic properties of nanostructured densified ferrimagnetic composites with grapheme-graphite fillers. *Mater. Des.* **2017**, *118*, 75–80. doi:10.1016/j.matdes.2017.01.018.
58. Kinsey, G.S.; Hebert, P.; Barbour, K.E.; Krut, D.D.; Cotal, H.L.; Sherif, R.A. Concentrator multijunction solar cell characteristics under variable intensity and temperature. *Prog. Photovolt. Res. Appl.* **2008**, *16*, 503–508. doi:10.1002/pip.834.
59. Chen, C.J. *Physics of Solar Energy*; Wiley: New York, NY, USA, 2011. doi:10.1002/9781118172841.
60. Markvart, T.; Castañer, L. *Practical Handbook of Photovoltaics: Fundamentals and Applications*. Elsevier: Amsterdam, Netherlands, 2003. doi:10.1016/B978-1-85617-390-2.X5000-4.
61. Radziemska, E. The effect of temperature on the power drop in crystalline silicon solar cells. *Renew. Energy Int. J.* **2003**, *28*, 1. doi:org/10.1016/S0960-1481(02)00015-0.
62. Singh, P.; Ravindra, N.M.; Temperature dependence of solar cell performance—an analysis. *Sol. Energy Mater. Sol. Cells.* **2012**, *101*, 36–45. doi:10.1016/j.solmat.2012.02.019.
63. Cheknane, A.; Benyoucef, B.; Chaker, A. Performance of concentrator solar cells with passive cooling. *Semicond. Sci. Technol.* **2006**, *21*, 144–147. doi:10.1088/0268-1242/21/2/007.
64. Anderson, W.G.; Dussinger, P.M.; Sarraf, D.B.; Tamanna, S. Heat Pipe Cooling of Concentrating Photovoltaic Cells. In Proceedings of the Photovoltaic Specialists Conference, PVSC '08, San Diego, CA, USA, 11–16 May 2008. doi:10.1109/PVSC.2008.4922577.
65. Yue, D.; You, F.; Darling, S.B. Domestic and overseas manufacturing scenarios of silicon-based photovoltaics: Life cycle energy and environmental comparative analysis. *Sol. Energy* **2014**, *105*, 669–678. doi:10.1016/j.solener.2014.04.008.



© 2017 by the authors. Submitted for possible open access publication under the terms and conditions of the Creative Commons Attribution (CC BY) license (<http://creativecommons.org/licenses/by/4.0/>).